Electronic and optical properties of hexathiapentacene in the gas and crystal phases

R. Cardia,[1,2] G. Malloci,[1,*] G.-M. Rignanese,[3] X. Blase,[4] E. Molteni,[5] and G. Cappellini[1,2,†]

[1]*Università degli Studi di Cagliari, Dipartimento di Fisica, Cittadella Universitaria, I-09042 Monserrato (Cagliari), Italy*

[2]*Istituto Officina dei Materiali (CNR-IOM), UOS di Cagliari, Cittadella Universitaria, I-09042 Monserrato (Cagliari), Italy*

[3]*Institute of Condensed Matter and Nanoscience (IMCN), Université Catholique de Louvain, B-1348 Louvain-la-neuve, Belgium*

[4]*CNRS and Grenoble-Alpes University, Institut Néel, F-38042 Grenoble, France*

[5]*Università degli Studi di Milano, Dipartimento di Fisica, Milano, Italy*

(Received 25 November 2015; revised manuscript received 27 May 2016; published 16 June 2016)

Using density functional theory (DFT) and its time-dependent (TD) extension, the electronic and optical properties of the hexathiapentacene (HTP) molecule, a derivative of pentacene (PNT) obtained by symmetric substitution of the six central H atoms with S atoms, are investigated for its gas and solid phases. For the molecular structure, all-electron calculations are performed using a Gaussian localized orbital basis set in conjunction with the Becke three-parameter Lee-Yang-Parr (B3LYP) hybrid exchange-correlation functional. Electron affinities, ionization energies, quasiparticle energy gaps, optical absorption spectra, and exciton binding energies are calculated and compared with the corresponding results for PNT, as well as with the available experimental data. The DFT and TDDFT results are also validated by performing many-body perturbation theory calculations within the GW and Bethe-Salpeter equation formalisms. The functionalization with S atoms induces an increase of both ionization energies and electron affinities, a sizable reduction of the fundamental electronic gap, and a redshift of the optical absorption onset. Notably, the intensity of the first absorption peak of HTP falling in the visible region is found to be nearly tripled with respect to the pure PNT molecule. For the crystal structures, pseudopotential calculations are adopted using a plane-wave basis set together with the Perdew-Burke-Ernzerhof exchange-correlation functional empirically corrected in order to take dispersive interactions into account. The electronic excitations are also obtained within a perturbative B3LYP scheme. A comparative analysis is carried out between the ground-state and excited-state properties of crystalline HTP and PNT linking to the findings obtained for the isolated molecules.

DOI: 10.1103/PhysRevB.93.235132

I. INTRODUCTION

Organic semiconductors based on polycyclic aromatic hydrocarbons (PAHs) are being widely used as active components in different kinds of devices such as organic field effect transistors (OFETs), organic light-emitting diodes (OLEDs), and organic photovoltaic (OPV) cells [1]. Linear acenes, in particular, are p-type semiconductors with good transport properties and are commonly employed as hole transporters in OFETs [2–4]. These devices consist of either single or multiple semiconducting parts which are usually assembled in layered (e.g., OFETs and OLEDs) or blended (e.g., OPV-bulk heterojunction) arrangements [5]. Small molecules offer several advantages in comparison to polymers: they can be easily purified by different techniques and processable by both evaporation and solution processing methods [6]. In addition, the electronic, optical, and transport properties of small PAHs can be fine-tuned via chemical modification or through the addition of functional groups to the conjugated core [2,7–10]. For example, the modification with strong electronegative substituents is an effective approach for converting p-type organic semiconductors to n type [2,11].

The performances of optoelectronic devices based on organic materials are known to depend on crystal structure and thin-film morphology. These properties therefore have been extensively studied in the past years, especially for nonfunctionalized and functionalized linear acenes and heterocyclic derivatives [12–16]. In particular, the face-to-face π-stacking motif is believed to be more efficient for charge transport than the edge-to-face herringbone-packing structures typical of organic semiconductors such as pentacene, rubrene, etc. [3,17]. It is known that the tendency to form face-to-face stacked structures can be enhanced by adding peripheral substituents [3,18]. Inspired from studies on tetrathiafulvalene derivatives whose transport properties are enhanced by the presence of S-S interactions [19,20], some groups have started introducing S atoms in the periphery of oligoacenes in order to provide an alternative charge transport pathway other than the "natural" π-π one [18,21].

Calculations of the electronic and optical properties of the building blocks of organic semiconductors can contribute to understanding their properties and can provide guidelines for future dedicated research [8,10]. A large number of theoretical studies on the properties of molecular materials have been published over the years [22–26]. The aim of this work is to theoretically evaluate the effect of S functionalization on the electronic and optical properties of a prototypical linear PAH in both gas and solid phases. We consider hexathiapentacene (HTP, $C_{22}H_8S_6$), a derivative of pentacene (PNT, $C_{22}H_{14}$) obtained by the symmetric substitution of six central H atoms with S atoms (a representation of the two molecules is given in Fig. 1).

HTP is an interesting compound with unusual molecular packing and remarkable properties. First described several years ago [27], this material has been extensively studied by Briseno and collaborators [18,28]. They first reported a band

*giuliano.malloci@dsf.unica.it

†giancarlo.cappellini@dsf.unica.it

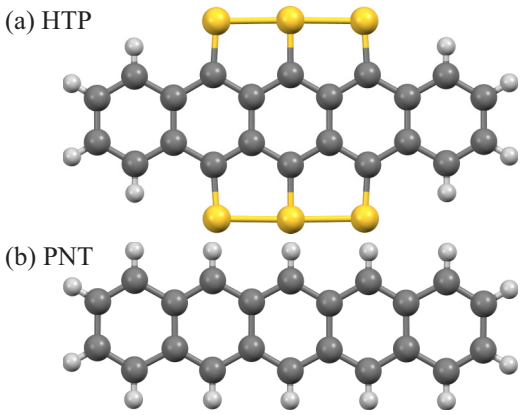

FIG. 1. Ball-and-stick representation of (a) hexathiapentacene (HTP) and (b) pentacene (PNT) molecules. The C, S, and H atoms are represented in grey, yellow, and white, respectively.

gap of about 1.63 eV (for the molecule in solution), a value which could be appealing for solar cell applications [18]. Then, HTP as a charge carrier of the order of $1 \times 10^{-2}\,\mathrm{cm}^2\,\mathrm{V}^{-1}\,\mathrm{s}^{-1}$ (measured for HTP nanowires) and a simple solution phase route for the synthesis of HTP nanowires were reported [28], opening the way to incorporate HTP as the semiconducting material in field effect transistors [28]. To the best of our knowledge, however, an extensive theoretical characterization of this material has not been reported so far.

We use density functional theory (DFT) [29] and time-dependent DFT (TDDFT) [30] to determine the effects of this particular substitution on the electronic and optical properties of HTP in comparison with PNT. In particular, we compare electron affinities, ionization energies, quasiparticle gaps, optical absorption spectra, and exciton binding energies. Finally, we also investigate the electronic properties of HTP and PNT molecular crystals within the DFT framework in both the ground state and the excited one.

II. COMPUTATIONAL METHODS

For the molecules, DFT calculations were performed using the NWCHEM package [31]. Following previous works [32–35] geometry optimization was carried out using the Becke three-parameter Lee-Yang-Parr (B3LYP) hybrid exchange-correlation functional [36–38], in combination with the 6-31+G* basis set, a valence double-ζ set augmented with d polarization functions and s and p diffuse functions. Extensive benchmark investigations performed in previous studies have shown that the B3LYP functional gives the overall best agreement with available experimental data for this class of molecules [32–34]. The equilibrium C-S distance was found to be 1.72 Å (1.75 Å for the central S atoms); this corresponds to an increase of 58% (61%) with respect to the corresponding C-H bond length in the PNT molecule. The other C-C and C-H lengths in the S-substituted molecules remained almost unchanged. The adiabatic electron affinities and ionization energies have been calculated via total energy differences. The vertical ionization energies (IE_V) and electron affinities (EA_V) have been evaluated at the relaxed geometry of the neutral molecules. This procedure enabled the calculations of the quasiparticle gap which is rigorously defined in the ΔSCF scheme as [39,40]

$$E_{\mathrm{gap}} = \mathrm{IE}_V - \mathrm{EA}_V = (E_{N+1} - E_N) - (E_N - E_{N-1}),$$

where E_N is the total energy of the N-electron system.

Using TDDFT, the excitation energies and the electronic absorption spectra in the visible and near-UV regions have also been obtained. The calculations were performed with the NWCHEM package adopting the same B3LYP/6-31+G* level of theory. We used the so-called Casida approach based on the linear response of the density matrix, in which the poles of the linear response function correspond to vertical excitation energies and the pole strengths to the corresponding oscillator strengths [41]. Knowing the first optically active transition E_{opt}, the exciton binding energy has been estimated through the difference $E_{\mathrm{bind}} = E_{\mathrm{gap}} - E_{\mathrm{opt}}$.

The DFT and TDDFT calculations are corroborated by many-body perturbation theory (MBPT) calculations within the GW and Bethe-Salpeter equation (BSE) formalisms [42], using the same geometries and basis set as that used at the DFT/TDDFT level. Our GW/BSE calculations are performed with the FIESTA package [43–45] and take as an input the same B3LYP/6-31+G* Kohn-Sham eigenstates as generated by the NWCHEM package, allowing comparison with the TD B3LYP calculations on equal footing. Following a recent benchmark study of the optical absorption energies of a large standard set of organic molecules [45], we perform partially self-consistent GW calculations, namely reinjecting self-consistently the corrected quasiparticle energies in the construction of the Green's function G and the screened Coulomb potential W. This was shown to lead to an excellent agreement with the so-called best theoretical estimates provided by high-level quantum chemistry techniques [45]. Our BSE calculations are performed beyond the Tamm-Dancoff approximation, namely mixing excitations and deexcitations. More details about the methodology can be found in Ref. [45].

For the crystal structures, all DFT calculations have been performed with the ABINIT code [46–48]. We employed Troullier-Martins pseudopotentials [49] and a plane-wave expansion of the wave functions using an energy cutoff E_{cut} of 50 Ry. The Brillouin zone (BZ) was sampled using a $4 \times 4 \times 4$ grid. The exchange-correlation (XC) energy was approximated using the Perdew-Burke-Ernzerhof (PBE) [50] generalized gradient approximation functional with the addition of the Grimme semiempirical D3 long-range dispersion correction [51] combined with Becke-Johnson damping [52].

The PNT and HTP unit cells are characterized by the triclinic space group $P\bar{1}$ and contain two molecules. They are displayed in Fig. 2. We relaxed both the atomic positions and the cell parameters by minimizing the forces acting on the atoms (reaching less than 1 meV/Å) and the stresses (reaching less than 1 kPa). The relaxed cell parameters (reported in Table I) are in excellent agreement (average error smaller than 1%) with the experimental values taken from Refs. [14] and [18] for PNT and HTP, respectively.

PNT and HTP show very similar H-H bonds (see distances d_1 and d_2 in Fig. 2) connecting the molecules along the long molecular axes. In contrast, the bonding between molecules in the other two directions is very different in PNT and HTP. In the former, H atoms are connected to C atoms (distances

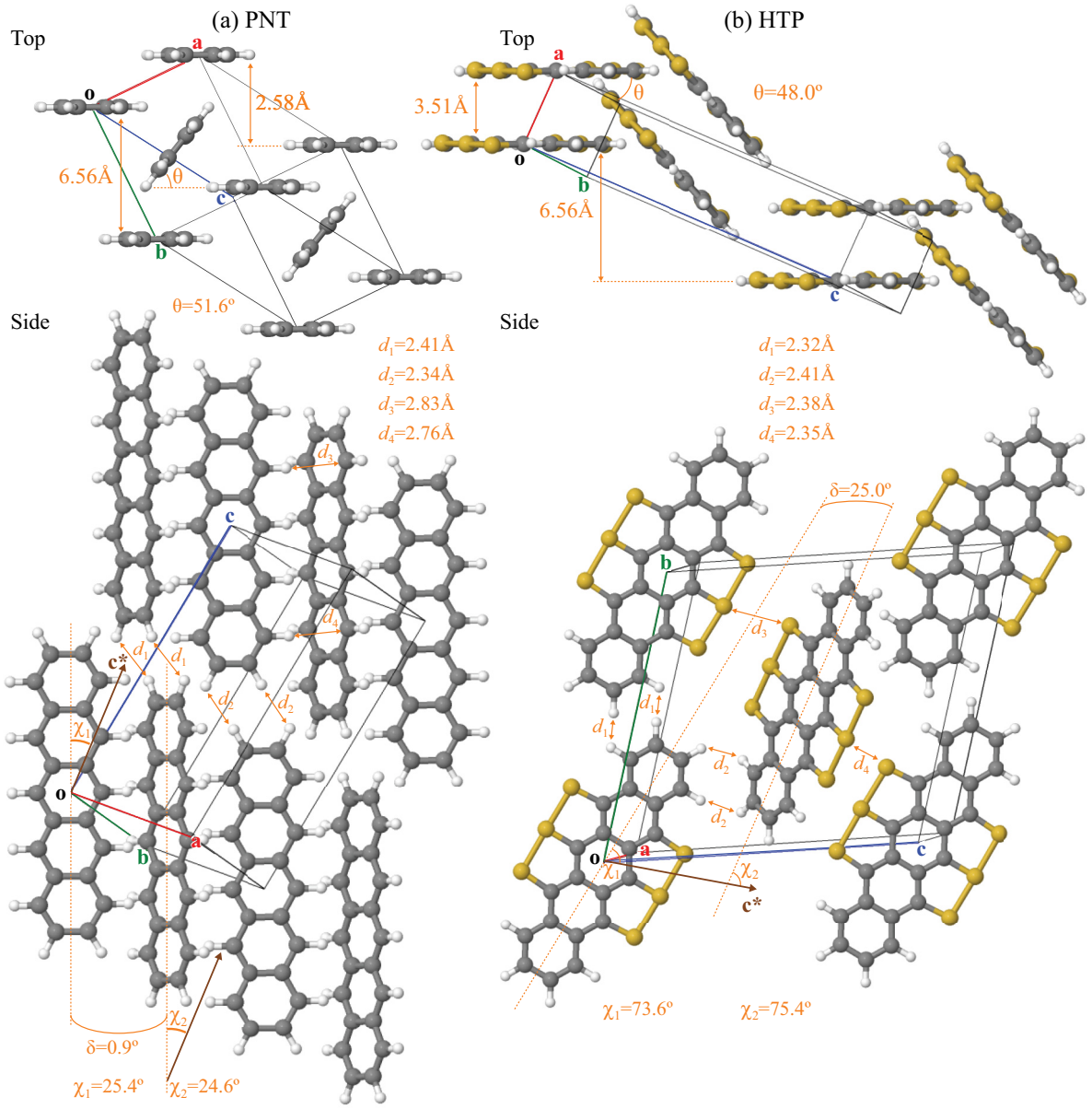

FIG. 2. Ball-and-stick representation of the unit cells of crystalline (a) PNT and (b) HTP. In the upper panels, the top view is reported parallel to the vector orthogonal to the two directions normal to the molecules. In the lower panels, the side view is generated such that one of the two molecules is in the plane. Various distances and angles (see text) are reported directly in the figure. Only selected repeated images are reproduced in order to ease the visual perception. The C, S, and H atoms are represented in grey, yellow, and white, respectively.

d_3 and d_4) whereas in the latter S-S bonds are formed, leading to a very different arrangement of the molecules in the two crystals. Both PNT and HTP exhibit a herringbone pattern with herringbone angles θ of 50°. Three more angles are used to describe the orientation of the molecules inside the crystal: δ, the angle between the long molecular axes; χ_1 and χ_2, the angles between each long molecular axis; and the reciprocal lattice vector $\mathbf{c}^*$ (which is perpendicular to lattice vectors **a** and **b**). In PNT, the long molecular axes of the molecules are nearly parallel to each other (δ is almost zero). This is very

TABLE I. Theoretical and experimental lattice parameters for the crystal structures of hexathiapentacene [18] and pentacene [14].

		a (Å)	b (Å)	c (Å)	α (deg)	β (deg)	γ (deg)
HTP	PBE	3.875	14.263	16.465	72.865	89.087	84.157
	Expt.	3.894	14.334	16.551	72.458	88.886	84.169
PNT	PBE	6.231	7.656	14.427	76.862	88.087	84.451
	Expt.	6.266	7.775	14.530	76.475	87.682	84.684

TABLE II. Calculated observables for HTP and PNT molecules: adiabatic and vertical electron affinities (EA_A, EA_V) and ionization energies (IE_A, IE_V), quasiparticle corrected HOMO-LUMO gaps (E_{gap}), optical gap (E_{opt}), and exciton binding energy (E_{bind}). The optical gap E_{opt} is obtained at the TDDFT or BSE level. The excitonic binding energy E_{bind} is the difference between E_{gap} and E_{opt}. All other theoretical results are obtained within DFT and B3LYP or GW. For the sake of brevity, we label the DFT and TDDFT (respectively GW and BSE) results as "DFT" (respectively "MBPT"). The experimental data from HTP and PNT are from Refs. [18] and [34]. All values are given in eV.

		IE_A	IE_V	EA_A	EA_V	E_{gap}	E_{opt}	E_{bind}
HTP	DFT	6.70	6.76	2.34	2.27	4.49	1.79	2.70
	MBPT		6.78		2.35	4.44	1.56	2.88
	Expt.						1.61	
PNT	DFT	6.12	6.16	1.48	1.41	4.75	1.91	2.84
	MBPT		6.42		1.48	4.95	1.84	3.11
	Expt.		6.59		1.39	5.20	1.91	2.89

different in HTP for which $\delta = 25^\circ$. The values of χ_1 and χ_2 are also very different in both cases.

The particular π-stacking structure of HTP can be ascribed to the sulfur atoms which prevent the edge-to-face interactions of the molecular units of PNT. In fact face-to-face stacking, which is believed to be more efficient in transport than the herringbone one, has been proven to be favored with added peripheral substituent atoms [18]. Moreover, the interchain distances (d_3 and d_4 in Fig. 2) are shorter in HTP than in PNT. This can be ascribed to the electrostatic intermolecular attraction between the partial positive charge of the outer S atoms with the partial negative charge of the central S atom of neighboring molecules [18].

For the electronic band structures, the electronic properties relying on the DFT eigenvalues lead to a well-known underestimation of the band gap in particular with semilocal functionals such as PBE [42,53–55]. MBPT calculations should in principle be performed. But this task is very demanding and beyond the scope of our study. Hybrid functionals have been proposed as a cheaper alternative approach to cure the band-gap problem. In recent studies [56,57], it was pointed out that, in solids, the inverse of the macroscopic dielectric constant provides a "reasonable" value for the fraction of exact exchange to be included in the hybrid functional. In organic crystals such as HTP and PNT, the typical dielectric constant is of the order of 4–5, leading empirically to 20% or 25% of exact exchange. This points to the well-known B3LYP functional that contains 20% of exact exchange. In the spirit of the single-shot G_0W_0 formalism, we have therefore performed a perturbative B3LYP correction [58] to the PBE electronic energies $\varepsilon_{n\mathbf{k}}^{\mathrm{PBE}}$ as

$$\varepsilon_{n\mathbf{k}}^{\mathrm{B3LYP}} = \varepsilon_{n\mathbf{k}}^{\mathrm{PBE}} + \left\langle \psi_{n\mathbf{k}}^{\mathrm{PBE}} \middle| V_{\mathrm{XC}}^{\mathrm{B3LYP}} - V_{\mathrm{XC}}^{\mathrm{PBE}} \middle| \psi_{n\mathbf{k}}^{\mathrm{PBE}} \right\rangle,$$

assuming that the PBE $\psi_{n\mathbf{k}}^{\mathrm{PBE}}$ are very close to the B3LYP ones. By using the B3LYP functional for both the molecular and crystal structures of PNT and HTP, they are treated on the same footing in terms of XC effects. For the sake of comparison, we also performed some calculations using the PBE0 [59,60] and Heyd-Scuseria-Ernzerhof (HSE) [61] functionals. The results (reported in the Supplemental Material [62]) highlight the limitations of the reliability of hybrid functionals as already discussed in the literature [63].

III. RESULTS AND DISCUSSION

A. Gas-phase electronic properties

The computed electronic properties for HTP and PNT molecules are reported in Table II together with the corresponding experimental data when available. The difference between theory and experiments is always below 8%, showing the accuracy of the computational procedure adopted. For the absolute values of the ionization energy (IE) and the electron affinity (EA), the aug-cc-pVTZ basis had to be used for the GW calculations. Indeed, they converge more slowly with basis size as compared to ΔSCF DFT calculations. Explicit comparisons between the 6-31+G* and aug-cc-pVTZ GW values confirm, however, that the highest occupied molecular orbital (HOMO)–lowest unoccupied molecular orbital (LUMO) gap is converged within 10 meV at the 6-31+G* level, indicating that occupied and unoccupied states are affected very similarly by basis-set changes.

With respect to the parent molecule the HTP shows an increase of IE by 10% ($\sim$ 0.6 eV for both the adiabatic and vertical quantities) and a sizable rise of EA up to 60% (about 0.86 eV for both vertical and adiabatic quantities). The quasiparticle gap (E_{gap}) is consequently reduced by 5.5% (0.26 eV). The optical absorption onset (E_{opt}) is found to be redshifted by about 6% (0.12 eV). The difference between this quantity and the E_{gap} provides an estimate of the exciton binding energy (E_{bind}) which appears to be reduced by 5% (0.14 eV).

Note that, to strengthen the comparison between data obtained with different methodologies, we checked for PNT that using the same computational scheme adopted for the solid phase, namely PBE and B3LYP applied perturbatively using ABINIT (vide infra), yields a reasonable agreement with the results obtained with NWCHEM. The comparison between the two methods is reported in the Supplemental Material [62].

B. Gas-phase optical properties

Figure 3 displays the absorption spectra in the visible region (in the energy range from 1.5 to 3.75 eV) of HTP and PNT as computed using the frequency-space implementation of TDDFT in NWCHEM. In particular, starting from the discrete set of computed electronic transitions E_i and their corresponding oscillator strengths f_i we obtained the dipole strength function $S(E)$, which has units of oscillator strength per unit energy and

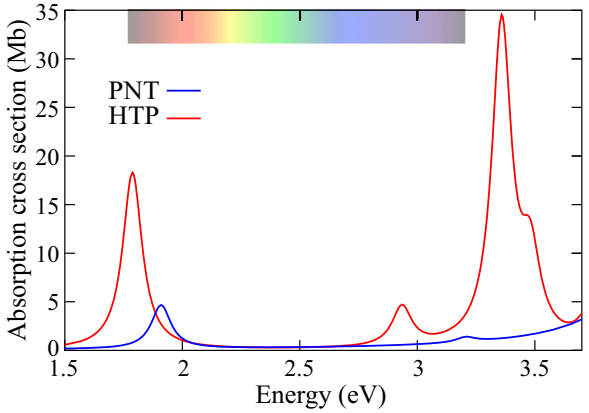

FIG. 3. Comparison between the computed TDDFT absorption cross section (in Mb) of molecular PNT (blue solid line) and HTP (red solid line) as a function of energy (in eV). Artificial broadening adopted: 0.07 eV.

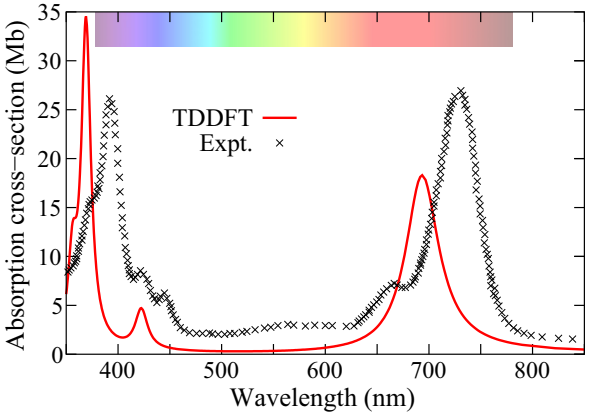

FIG. 4. Comparison between the computed TDDFT (red solid line) and experimental (black crosses) absorption cross section (in Mb) of molecular HTP as a function of the wavelength (in nm). The experimental data are taken from Ref. [18].

satisfies the dipole sum rule $N_e = \int dE\, S(E)$, where N_e is the total number of electrons. Our spectra are reported in terms of the absorption cross section $\sigma(E)$, which is related to the dipole strength function $S(E)$ by the equation

$$S(E) = \frac{m_e c}{\pi h e^2}\sigma(E), \tag{1}$$

where h is Planck's constant, c is the velocity of light in vacuum, and m_e and e are the mass and charge of the electron, respectively.

For the energy range considered, PNT shows only a very small absorption peak (4.7 Mb) at 1.91 eV and is almost inactive in the remaining part of the visible range. At variance with PNT, HTP shows a redshift of the optical onset (with a reduction of −0.12 eV) with an enhancement of this absorption structure, the amplitude of which rises up to 18 Mb. A second small absorption peak (4.7 Mb of amplitude) appears at the upper side of the visible region (more specifically at 2.93 eV). The substituted compound shows its most important absorption structure at the lower edge of the near-UV region. This structure presents a main peak (34.5 Mb of amplitude) at 3.35 eV and a shoulder (13.9 Mb) at 3.46 eV.

With respect to the unsubstituted molecule, HTP globally presents an increasing of absorption in the visible region, due to a combination of increased amplitude of the first absorption peak and a new structure at the upper edge of the visible region. The S-functionalized molecule also presents its most important absorption peak in the very near UV range of energies, in which pentacene does not show absorption peaks.

Figure 4 shows the comparison between our TDDFT calculated spectrum and the experimental absorption spectrum of hexathiapentacene taken in solution with 1,2-dichlorobenzene at 100°C [18]. We found reasonably good agreement in terms of the position of the main absorption peaks, with a blueshift of ∼5% of the theoretical peaks with respect to the experimental ones. The experimental peak (A) at 391.8 nm (3.16 eV) is shifted by 22.7 nm at 369.1 nm (3.36 eV), while the experimental peak (B) at 730.9 nm (1.7 eV) is shifted by 37.4 nm at 693.5 nm (1.79 eV). These differences are mainly due to known effects of the solvent on the measured absorption spectra [64].

The computed and experimental absorption peaks should also be considered in terms of the effective oscillator strengths, which are proportional to the area beneath the reported structures. The experimental peaks A and B have an area of 530 Mb nm and 1613 Mb nm (which correspond to oscillator strengths of 0.20 and 0.59, respectively), while the theoretical ones show an area of 455 Mb nm and 820 Mb nm (i.e., oscillator strengths of 0.17 and 0.30, respectively). The agreement is thus much better in the high-energy structure with a difference of 16% for peak A to be compared to 49% for peak B (at lower energy).

In Figs. 5 and 6, we reported the comparison of the absorption spectra calculated within TDDFT and the GW-BSE method in both cases using the basis set 6-31+G*. In Fig. 5, the use of the GW-BSE method produces a principal peak at 4.26 eV nearly coincident with that of TDDFT (aside from a 21% reduction in intensity) and a blueshifted small structure at the onset around 2 eV. In Fig. 6, the two peaks around 2.9 and 3.4 eV produced by the two methods almost coincide. On

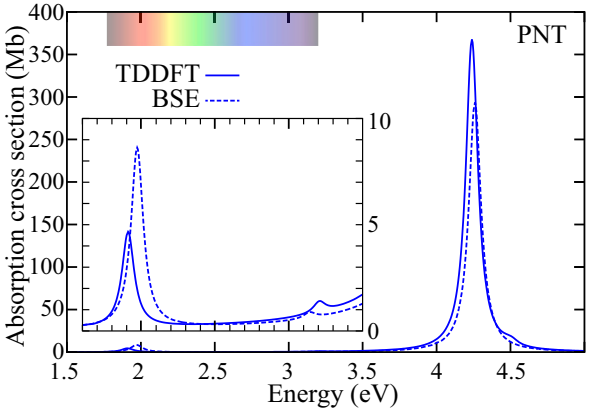

FIG. 5. Comparison between the computed TDDFT (blue solid line) and BSE (blue dashed line) absorption cross section (in Mb) of molecular PNT as a function of the energy (in eV).

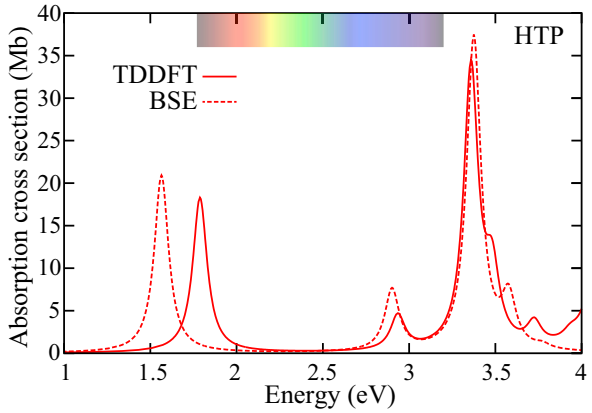

FIG. 6. Comparison between the computed TDDFT (red solid line) and BSE (red dashed line) absorption cross section (in Mb) of molecular HTP as a function of the energy (in eV).

the other hand, the GW-BSE scheme describes an absorption peak onset redshifted by 0.23 eV as compared to TDDFT.

Again, to strengthen the comparison between data obtained with different methodologies and to give additional consistency to our results for the gas phase, we checked the agreement between the results described above for PNT with the BSE data obtained with the ABINIT code used for the solid phase. The comparison is reported in the Supplemental Material [62].

C. Solid-phase electronic properties

The electronic band structures for the solid phases of HTP and PNT have been calculated along the high-symmetry lines of the BZ. They are reproduced in Fig. 7 following the conventions of Ref. [65]. The subbands corresponding to the uppermost valence-band pair and lowest conduction-band pair are represented in blue and red, respectively. The fundamental gap is located at the N point for PNT and at the X point for HTP at B3LYP level (see Table III and following lines). We report in the last row of Table III previous PBE results for PNT [66], which show only small differences, within 2.7%, with respect to our data. In addition the fundamental gap here obtained compares fairly well (difference within 2.7%) with the one recently reported adopting the same computational scheme [24].

The band structures obtained with the PBE functional (solid lines) exhibit the well-known band-gap problem of DFT [42,53–55]. For PNT, the calculated gap of 0.73 eV is considerably smaller than the experimental values of 2.2–2.4 eV [66]. Using the B3LYP functional (dashed lines), it reaches 1.60 eV which is a clear improvement but still 0.6–0.8 eV below the experimental value. Note that the calculated GW [67] quasiparticle gap of 1.9 eV is also 0.3–0.5 eV too low. For HTP, the PBE gap is 1.03 eV while the B3LYP value is 1.95 eV. We are not aware of any measurement or of any GW calculations. However, we expect that a similar trend also holds with $E_{\rm gap}^{\rm B3LYP} < E_{\rm gap}^{GW} < E_{\rm gap}^{\rm expt}$.

For PNT, the fundamental gap (at the N point) is only 10 meV smaller than the direct interband transition at the L point within both PBE and B3LYP. For HTP, the fundamental gap (at the X point) is almost equal to the direct interband transition at the Γ point within PBE, but it is 10 meV smaller within B3LYP. Since the experimental error on the band gap is typically of the order of 100 meV [66], we expect that the above transitions can hardly be resolved by the measurements.

It is important to consider that, while, in the gas phase, the fundamental gap of HTP is smaller than the one of PNT,

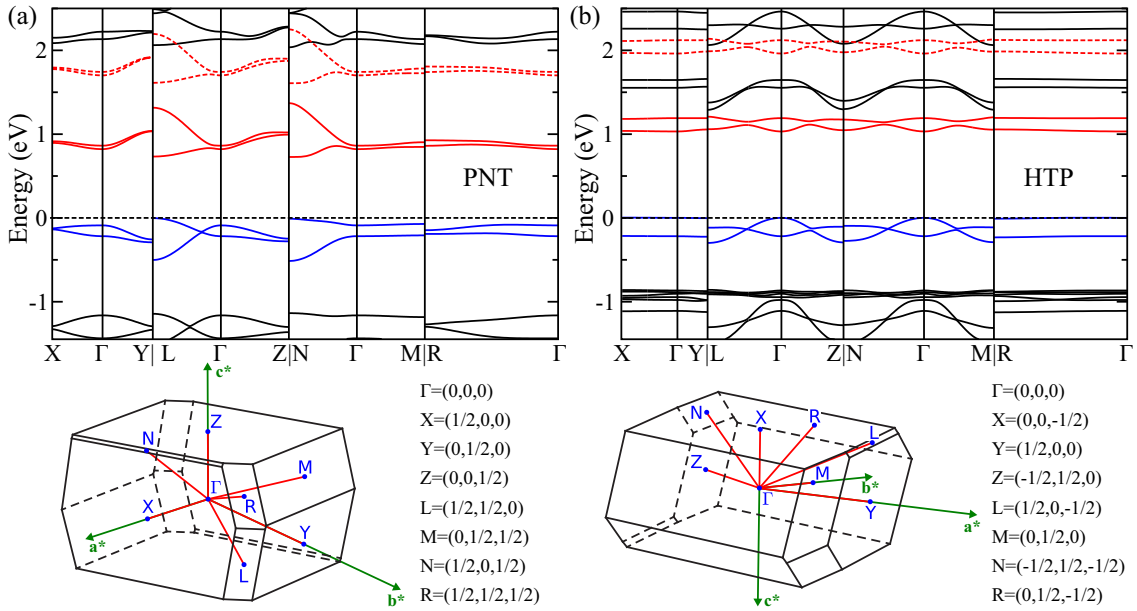

FIG. 7. Electronic band structure of the crystalline structures of (a) PNT and (b) HTP at PBE (solid lines) and perturbative B3LYP (dashed lines) levels. The subbands corresponding to the uppermost valence-band pair and lowest conduction-band pair are highlighted in blue and red, respectively. The horizontal black dotted line represents the valence band maximum set as the energy zero. Dashed blue lines are overlapped to the corresponding solid blue lines. The corresponding Brillouin zones and high-symmetry points are also reported following the conventions of Ref. [65].

TABLE III. Direct interband transition at the high-symmetry points for solid HTP and PNT calculated within PBE and B3LYP. Previous PBE results from Ref. [66] are also reported for PNT. All values are given in eV.

	Γ	X	Y	Z	L	M	N	R
HTP (this work)								
PBE	1.03	1.03	1.06	1.15	1.18	1.17	1.14	1.06
B3LYP	1.96	1.95	1.99	2.09	2.12	2.11	2.08	1.99
PNT (this work)								
PBE	0.91	1.03	1.29	1.24	0.74	0.92	0.73	1.01
B3LYP	1.80	1.93	2.26	2.21	1.61	1.81	1.60	1.91
PNT (from Ref. [66])								
PBE	0.89	1.03	1.29		0.72	0.92	0.71	

the trend is reversed in the solid phase. However, the bands are more dispersive in PNT than in HTP (see Supplemental Material [62]). And, if we consider the direct transitions in the different high-symmetry points of the Brillouin zone, the largest value is obtained in PNT (see Supplemental Material [62]). This difference of behavior can probably be ascribed to the different molecular packing and interaction (due to the S atoms) in the two crystals. However, no clear trend emerges when trying to rationalize the dispersion of the bands along the different high-symmetry lines in terms of their projection onto the long, short, and normal directions for the two molecules in the unit cells of PNT and HTP (see Supplemental Material [62]). Our findings show that the trends found in the gas phase do not necessarily hold in the solid phase.

IV. CONCLUSIONS

We have presented a comparative investigation between the electronic properties of isolated molecules and the corresponding molecular solids in the specific case of hexathiapentacene and pentacene using state-of-the-art computational techniques. We have studied how molecular features are modified within the solid environment.

For the molecular phase using an all-electron code, we have computed ionization energies, electron affinities, quasiparticle gap, optical absorption spectra, and exciton binding energies. We have found larger electron affinities and ionization energies for HTP, as compared to its parent PNT molecule, which give rise to a reduction of the quasiparticle gap. The onset energy of the optical absorption spectrum for the molecules is redshifted following functionalization and the same trend is found for the exciton binding energy. The visible and near-UV region of the HTP molecular spectrum shows an enhancing of the absorption due to the redshift and increased amplitude of the first peak and due to the new large structures in the very near UV region.

For the corresponding PNT and HTP crystalline molecular solids, we have observed that different molecular packing and sulfur substitution determine important differences in the electronic properties of the two systems. We have found that the dispersion of the bands is particularly different in the two solids. Moreover, we found an inversion of the band-gap ordering between the gas and solid phases of the two molecules.

ACKNOWLEDGMENTS

R.C. gratefully acknowledges the Sardinia Regional Government for the financial support of his Ph.D. scholarship (P.O.R. Sardegna F.S.E. Operational Programme of the Autonomous Region of Sardegna, European Social Fund 2007.2013, Axis IV Human Resources, Objective I.3, Line of Activity I.3.1). G.C. acknowledges financial support from Regione Autonoma della Sardegna under Project RAS L.R. No. 07/08/2007 CRP-26666. G.C. and R.C. also acknowledge financial support from IDEA-AISBL (Bruxelles, Belgium) and computational support by CINECA through the ISCRA Initiative (Project PAHMOS). G.-M.R. acknowledges financial support from the F.R.S.-FNRS and access to various computational resources: the Tier-1 supercomputer of the Fédération Wallonie-Bruxelles funded by the Walloon Region (Grant No. 1117545), and all the facilities provided by the Université Catholique de Louvain (CISM/UCL) and by the Consortium des Équipements de Calcul Intensif en Fédération Wallonie Bruxelles (CÉCI). X.B. acknowledges funding from the French National Science Funding agency under Contract No. ANR-12-BS04 "PANELS" and from the European Union under Contract No. H2020-EU.2.1.3.1 "EXTMOS" and access to the CURIE supercomputing facilities thanks to the GENCI program.

[1] B. Lucas, T. Trigaud, and C. Videlot-Ackermann, Polym. Int. **61**, 374 (2012).
[2] A. L. Appleton, S. M. Brombosz, S. Barlow, J. S. Sears, J. Bredas, S. R. Marder, and U. H. F. Bunz, Nat. Commun. **1**, 91 (2010).
[3] J. E. Anthony, Chem. Rev. **106**, 5028 (2006).
[4] J. E. Anthony, Angew. Chem. Int. Ed. **47**, 452 (2008).
[5] H. Ma, H.-L. Yip, F. Huang, and A. K.-Y. Jen, Adv. Funct. Mater. **20**, 1371 (2010).
[6] K. B. Burke, Y. Shu, P. Kemppinen, B. Singh, M. Bown, I. I. Liaw, R. M. Williamson, L. Thomsen, P. Dastoor, W. Belcher, C. Forsyth, K. N. Winzenberg, and G. E. Collis, Cryst. Growth Des. **12**, 725 (2012).
[7] H. Sun, A. Putta, and M. Billion, J. Phys. Chem. A **116**, 8015 (2012).
[8] O. Lobanova Griffith, N. E. Gruhn, J. E. Anthony, B. Purushothaman, and D. L. Lichtenberger, J. Phys. Chem. C **112**, 20518 (2008).
[9] X. Feng, Q. Li, J. Gu, F. A. Cotton, Y. Xie, and H. F. Schaefer, J. Phys. Chem. A **113**, 887 (2009).
[10] O. Lobanova Griffith, J. E. Anthony, A. G. Jones, and D. L. Lichtenberger, J. Am. Chem. Soc. **132**, 580 (2010).
[11] M. L. Tang and Z. Bao, Chem. Mater. **23**, 446 (2011).
[12] M. Pedio, B. Doyle, N. Mahne, A. Giglia, F. Borgatti, S. Nannarone, S. Henze, R. Temirov, F. Tautz, L. Casalis, R. Hudej, M. Danisman, and B. Nickel, Appl. Surf. Sci. **254**, 103 (2007).

[13] H. Yang, T. J. Shin, M.-M. Ling, K. Cho, C. Y. Ryu, and Z. Bao, J. Am. Chem. Soc. **127**, 11542 (2005).

[14] C. C. Mattheus, A. B. Dros, J. Baas, A. Meetsma, J. L. de Boer, and T. T. M. Palstra, Acta Crystallogr. Sect. C **57**, 939 (2001).

[15] C. C. Mattheus, A. B. Dros, J. Baas, G. T. Oostergetel, A. Meetsma, J. L. de Boer, and T. T. Palstra, Synth. Met. **138**, 475 (2003).

[16] S. C. B. Mannsfeld, A. Virkar, C. Reese, M. F. Toney, and Z. Bao, Adv. Mater. **21**, 2294 (2009).

[17] F. Anger, R. Scholz, E. Adamski, K. Broch, A. Gerlach, Y. Sakamoto, T. Suzuki, and F. Schreiber, Appl. Phys. Lett. **102**, 013308 (2013).

[18] A. L. Briseno, Q. Miao, M.-M. Ling, C. Reese, H. Meng, Z. Bao, and F. Wudl, J. Am. Chem. Soc. **128**, 15576 (2006).

[19] M. Mas-Torrent, M. Durkut, P. Hadley, X. Ribas, and C. Rovira, J. Am. Chem. Soc. **126**, 984 (2004).

[20] M. Mas-Torrent and C. Rovira, J. Mater. Chem. **16**, 433 (2006).

[21] M. Bendikov, F. Wudl, and D. F. Perepichka, Chem. Rev. **104**, 4891 (2004).

[22] W. Perger, Chem. Phys. Lett. **368**, 319 (2003).

[23] M. A. L. Marques, A. Castro, G. Malloci, G. Mulas, and S. Botti, J. Chem. Phys. **127**, 014107 (2007).

[24] S. Sharifzadeh, A. Biller, L. Kronik, and J. B. Neaton, Phys. Rev. B **85**, 125307 (2012).

[25] A. Fonari, C. Sutton, J.-L. Brédas, and V. Coropceanu, Phys. Rev. B **90**, 165205 (2014).

[26] D. H. P. Turban, G. Teobaldi, D. D. O'Regan, and N. D. M. Hine, Phys. Rev. B **93**, 165102 (2016).

[27] E. P. Goodings, D. A. Mitchard, and G. Owen, J. Chem. Soc. Perkin Trans. **1**, 1310 (1972).

[28] A. L. Briseno, S. C. B. Mannsfeld, X. Lu, Y. Xiong, S. A. Jenekhe, Z. Bao, and Y. Xia, Nano Lett. **7**, 668 (2007).

[29] W. Kohn, Rev. Mod. Phys. **71**, 1253 (1999).

[30] M. Marques and E. Gross, Annu. Rev. Phys. Chem. **55**, 427 (2004).

[31] M. Valiev, E. J. Bylaska, N. Govind, K. Kowalski, T. P. Straatsma, H. J. J. Van Dam, D. Wang, J. Nieplocha, E. Apra, T. L. Windus, and W. A. de Jong, Comput. Phys. Commun. **181**, 1477 (2010).

[32] G. Malloci, G. Mulas, G. Cappellini, and C. Joblin, Chem. Phys. **340**, 43 (2007).

[33] G. Cappellini, G. Malloci, and G. Mulas, Superlattices Microstruct. **46**, 14 (2009).

[34] G. Malloci, G. Cappellini, G. Mulas, and A. Mattoni, Chem. Phys. **384**, 19 (2011).

[35] R. Cardia, G. Malloci, A. Mattoni, and G. Cappellini, J. Phys. Chem. A **118**, 5170 (2014).

[36] A. D. Becke, J. Chem. Phys. **98**, 5648 (1993).

[37] C. Lee, W. Yang, and R. G. Parr, Phys. Rev. B **37**, 785 (1988).

[38] P. J. Stephens, P. J. Devlin, C. F. Chabalowski, and M. J. Frisch, J. Phys. Chem. **98**, 11623 (1994).

[39] R. O. Jones and O. Gunnarsson, Rev. Mod. Phys. **61**, 689 (1989).

[40] G. Malloci, G. Cappellini, G. Mulas, and G. Satta, Phys. Rev. B **70**, 205429 (2004).

[41] M. E. Casida, in *Recent Advances in Density Functional Theory: Vol. I*, edited by D. P. Chong (World Scientific, Singapore, 1995).

[42] G. Onida, L. Reining, and A. Rubio, Rev. Mod. Phys. **74**, 601 (2002).

[43] X. Blase, C. Attaccalite, and V. Olevano, Phys. Rev. B **83**, 115103 (2011).

[44] X. Blase and C. Attaccalite, Appl. Phys. Lett. **99**, 171909 (2011).

[45] D. Jacquemin, I. Duchemin, and X. Blase, J. Chem. Theory Comput. **11**, 3290 (2015).

[46] X. Gonze, B. Amadon, P.-M. Anglade, J.-M. Beuken, F. Bottin, P. Boulanger, F. Bruneval, D. Caliste, R. Caracas, M. Côté, T. Deutsch, L. Genovese, P. Ghosez, M. Giantomassi, S. Goedecker, D. Hamann, P. Hermet, F. Jollet, G. Jomard, S. Leroux, M. Mancini, S. Mazevet, M. Oliveira, G. Onida, Y. Pouillon, T. Rangel, G.-M. Rignanese, D. Sangalli, R. Shaltaf, M. Torrent, M. Verstraete, G. Zerah, and J. Zwanziger, Comput. Phys. Commun. **180**, 2582 (2009).

[47] X. Gonze, G.-M. Rignanese, M. Verstraete, J.-M. Beuken, Y. Pouillon, R. Caracas, F. Jollet, M. Torrent, G. Zerah, M. Mikami, P. Ghosez, M. Veithen, J.-Y. Raty, V. Olevano, F. Bruneval, L. Reining, R. Godby, G. Onida, D. R. Hamann, and D. C. Allan, Z. Kristallogr. Cryst. Mater. **220**, 558 (2005).

[48] X. Gonze, J.-M. Beuken, R. Caracas, F. Detraux, M. Fuchs, G.-M. Rignanese, L. Sindic, M. Verstraete, G. Zerah, F. Jollet, M. Torrent, A. Roy, M. Mikami, P. Ghosez, J.-Y. Raty, and D. Allan, Comput. Mater. Sci. **25**, 478 (2002).

[49] N. Troullier and J. L. Martins, Phys. Rev. B **43**, 1993 (1991).

[50] J. P. Perdew, K. Burke, and M. Ernzerhof, Phys. Rev. Lett. **77**, 3865 (1996).

[51] S. Grimme, J. Antony, S. Ehrlich, and S. Krieg, J. Chem. Phys. **132**, 154104 (2010).

[52] S. Grimme, S. Ehrlich, and L. Goerigk, J. Comput. Chem. **32**, 1456 (2011).

[53] M. S. Hybertsen and S. G. Louie, Phys. Rev. B **34**, 5390 (1986).

[54] R. W. Godby, M. Schlüter, and L. J. Sham, Phys. Rev. B **37**, 10159 (1988).

[55] F. Bechstedt, R. Del Sole, G. Cappellini, and L. Reining, Solid State Commun. **84**, 765 (1992).

[56] M. A. L. Marques, J. Vidal, M. J. T. Oliveira, L. Reining, and S. Botti, Phys. Rev. B **83**, 035119 (2011).

[57] J. H. Skone, M. Govoni, and G. Galli, Phys. Rev. B **89**, 195112 (2014).

[58] As of today, the implementation of self-consistent B3LYP in ABINIT has not been optimized. Therefore, the required computational time is rather large and we decided to avoid such calculations.

[59] J. P. Perdew, M. Ernzerhof, and K. Burke, J. Chem. Phys. **105**, 9982 (1996).

[60] C. Adamo and V. Barone, J. Chem. Phys. **110**, 6158 (1999).

[61] J. Heyd, G. E. Scuseria, and M. Ernzerhof, J. Chem. Phys. **118**, 8207 (2003).

[62] See Supplemental Material at http://link.aps.org/supplemental/10.1103/PhysRevB.93.235132 for additional crystal phase electronic properties and comparison of different computational techniques.

[63] M. Jain, J. R. Chelikowsky, and S. G. Louie, Phys. Rev. Lett. **107**, 216806 (2011).

[64] D. Varsano, R. Di Felice, M. A. L. Marques, and A. Rubio, J. Phys. Chem. B **110**, 7129 (2006).

[65] W. Setyawan and S. Curtarolo, Comput. Mater. Sci. **49**, 299 (2010).

[66] K. Hummer and C. Ambrosch-Draxl, Phys. Rev. B **72**, 205205 (2005).

[67] M. L. Tiago, J. E. Northrup, and S. G. Louie, Phys. Rev. B **67**, 115212 (2003).